IEEE Access
Multidisciplinary | Rapid Review | Open Access Journal

Received September 28, 2020, accepted October 7, 2020, date of publication October 12, 2020, date of current version October 26, 2020.

Digital Object Identifier 10.1109/ACCESS.2020.3030268

Multilayer Spindle Shaped Magnetic Shielding Device for SERF Atomic Magnetometer Application

ZHENGKUN FAN, JUN XU, XIANGYU KANG, ZHANFEI ZHANG, YANG LI, XIANGMEI DONG, AND XIUMIN GAO

School of Optoelectronic Information and Computer Engineering, University of Shanghai for Science and Technology, Shanghai 200093, China

Corresponding author: Yang Li (liyang@usst.edu.cn)

This work was supported by the National Key Research and Development Plan through the Earth Observation and Navigation Key Special Project under Grant 2017YFB0503102.

ABSTRACT Most of shielding devices currently used for SERF magnetometers are multilayer cylindrical magnetic shielding barrels. This article studies a new multilayer spindle shaped magnetic shielding barrel for the spin exchange relaxation free (SERF) magnetometer shielding system and uses finite element method (FEM) to compare the analysis results. The results show that the shielding effect of the spindle shaped magnetic shielding barrel is better than the traditional cylindrical magnetic shielding barrel, while the volume is reduced by about 1/5 and the weight is reduced by about 1/4. Therefore, we expect that a small-sized, light-weight, low-cost and more efficient magnetic shielding device can be obtained.

INDEX TERMS Atomic magnetometer, spindle shaped, magnetic shielding, SERF.

I. INTRODUCTION

Highly sensitive magnetic field sensors have a wide range of applications in fields such as space science, detection technology, magnetic metrology, geomagnetic navigation, and weak magnetic biology [1]–[9]. An atomic magnetometer operating in the spin-exchange relaxation-free (SERF) regime has achieved the highest sensitivity in low-frequency magnetic field measurement —— 0.16 fT / $Hz^{1/2}$ [10]. The SERF magnetometer needs to work in SERF regime which requires efficient laser pumping, weak magnetic fields environment and uniform high temperature environment [11]–[13]. Laser pumping technology achieves the spin polarization of alkali metal atoms, so that the alkali metal atomic spin direction is consistent; the weak magnetic field environment is the precondition of the atomic SERF regime, while the uniform high temperature environment is for high density and even distribution of alkali metal atoms. However, the stray magnetic field in the environment would cause the atomic transition frequency to drift, thereby it reduces the performance of SERF magnetometers [14], [15]. In order to achieve ultra-sensitive magnetic field measurement, the relaxation of alkali metal atoms must be fully inhibited. It is an effective method to reduce the magnetic field in the atomic gas chamber using magnetic shielding, which can not only shield the external stray magnetic field, but also reduce the ambient magnetic field noise, magnetic field gradient and field offset [16]. Therefore, during the development of a high-sensitivity atomic magnetometer, for avoiding interference with the specific magnetic field needing in the experimental study, the external stray magnetic field must be shielded [17], [18]. The passive magnetic shielding device can shield the internal magnetic field to a stable space of almost zero field. According to the actual research situation or application requirements, ferromagnetic materials with high magnetic permeability are usually made into spherical shells or cylindrical barrels. In this way, the interference of external magnetic field to sensitive sensors can be effectively shielded [19]–[21].

In practical applications, the shielding device cannot be completely closed. From the perspective of metal fabrication and processing, cylindrical shape is easiest to manufacture, thus becoming the most used design structure [22]. The spindle shaped magnetic shielding barrel has more advantages than the cylindrical magnetic shielding barrel. Spindle shape is easier to manufacture than spheres [23]. In this article,

The associate editor coordinating the review of this manuscript and approving it for publication was Jenny Mahoney.

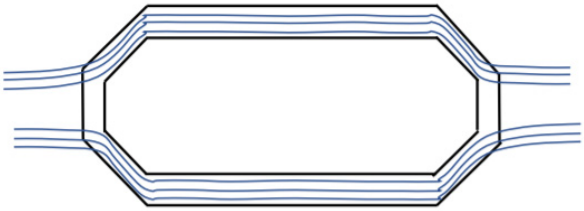

FIGURE 1. Magnetic field distribution around the magnetic shielding device.

a spindle shaped magnetic shielding barrel model is proposed, based on the optimization design of the cylindrical magnetic shielding barrel. When the total axial length is constant, the two models are compared by finite element analysis and spindle-shaped magnetic shielding barrel provide better shielding, the noise generated by both magnetic shielding barrels is about 15fT / $Hz^{1/2}$. Making the two ends of the shield barrel into a spindle shape can reduce the volume of the shield barrel by about 1/5 and the weight by about 1/4.

II. MAGNETIC SHIELDING THEORY AND MODEL ESTABLISHMENT

The principle of magnetic shielding can be explained with the concept of a parallel magnetic circuit. As shown in FIGURE. 1, when the magnetic shielding device is placed in the external magnetic field, the wall of the shielding shell and the air in the cavity surrounded can be regarded as parallel magnetic circuit. The magnetic permeability of air is close to the vacuum permeability $\mu_0 = 4\pi \times 10^{-7} \mathrm{N/A}^2$, while the magnetic permeability of the shielding device is much larger than 1. The magnetic resistance of the cavity is much larger than that of the shielding device.

The evaluation indexes of shielding effectiveness of magnetic shielding device include magnetic shielding coefficient S and magnetic shielding effectiveness S_E:

$$S = \frac{H_{\text{out}}}{H_{\text{in}}} \tag{1}$$

$$S_E = 20 \log S \tag{2}$$

where: H_{in} and H_{out} are the magnetic field strength inside and outside of the shield [25].

A. MAGNETIC SHIELDING MODEL

There are differences in the shape and size of the axial section and the radial section of the magnetic shielding barrel. The magnetic shielding barrel has axial and radial shielding coefficients.

The radial shielding coefficient S_t of the single-layer magnetic shielding barrel is:

$$S_{\text{t}} \approx 1 + \frac{1}{4}\mu_r[1 - (\frac{R_{in}}{R_{out}})^2] \tag{3}$$

where: μ_r is the relative permeability of the material, R_{in} and R_{out} are the internal and external radii of the cross-section circle of the shielding barrel respectively [25].

The axial shielding coefficient S_a of single-layer magnetic shielding barrel is:

$$S_{\text{a}} = \frac{1 + 4NS_t}{1 + R/L} \tag{4}$$

where: R is the average value of R_{in} and R_{out}, L is the inner length of single-layer magnetic shielding barrel, N is the demagnetization factor which is expressed:

$$N = [\frac{1}{(p^2-1)}]\{\frac{p}{(p^2-1)^{\frac{1}{2}}}\}\mathrm{In}[p + (p^2-1)^{\frac{1}{2}}] - 1\} \tag{5}$$

where: the parameter $\mathrm{p} = \frac{L}{2R}$, generally $1 < p < 40$ [26].

According to (3) and (4), the radial magnetic shielding coefficient of the magnetic shielding barrel is several times larger than the axial magnetic shielding coefficient, so the axial magnetic shielding coefficient is the main factor that limit the magnetic shielding effect of the magnetic shielding barrel.

The shielding coefficient of multilayer magnetic shielding barrel is S_{tot}:

$$S_{tot} = S_n \prod_{i=1}^{n-1} S_i[1 - (\frac{R_i}{R_i + 1})^{\mathrm{j}}] \tag{6}$$

where: R_i represent the magnetic shielding coefficient and radius of the i-th layer respectively. It is stipulated that R_i is smaller than R_{i+1}. When $j = 1$, S_{tot} represents the axial shielding coefficient of the single-layer. magnetic shield barrel. The length L_i of the shielding barrel replaces R_i from (6). When $j = 2$, S_{tot} represents the radial shielding coefficient of the multilayer shielding barrel [25].

B. MAGNETIC NOISE ANALYSIS

In SERF magnetometers, the noise generated in magnetic shielding devices is generally dominated by Johnson magnetic noise. Johnson magnetic noise is caused by the thermal motion of free electrons present in the material. Usually the material has excellent conductivity. Therefore, there is inevitable magnetic noise. The magnetic noise of the common mu-metal magnetic shield is mainly dominated by Johnson magnetic noise B_{jms}

$$B_{jms} = \frac{\mu_r \sqrt{kT\sigma t}}{r}\sqrt{\frac{2G}{3\pi}} \tag{7}$$

where: μ_r is the relative magnetic conductivity; k is the Boltzmann constant; T is the temperature; σ is the conductivity; t is the thickness of the magnetic shield; r is the radius of the magnetic shield; G is a constant related to the aspect ratio of magnetic shielded shapes [17], [18], [26], [27].

C. SERF ATOMIC MAGNETOMETER AND MAGNETIC SHIELD DESIGN

As shown in FIGURE.2, the alkali metal gas chamber is the core component of the SERF magnetometer. During the detection process, we need magnetic shielding to prevent interference from external factors. The pattern of magnetic

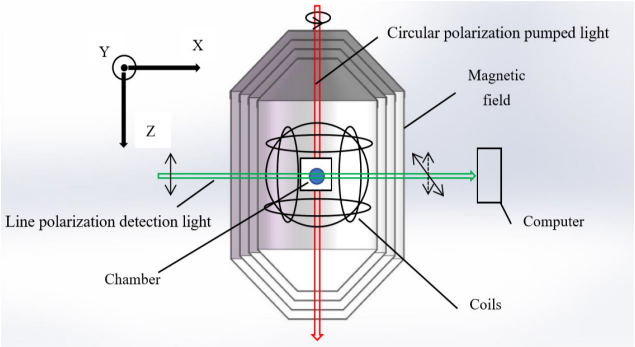

FIGURE 2. Essential composition and schematic diagram of the SERF atomic magnetometer.

TABLE 1. Size parameters of cylindrical magnetic shielding barrel.

Parameter name	Parameter value
Innermost axis length	250 mm
Innermost radius	65 mm
Axial length difference between two adjacent layers	10 mm
Radius difference between two adjacent layers	10 mm
Layer thickness	0.4 mm
Number of layers	4

shielding consists of two parts. One is the active magnetic compensation coil. The other is a high-performance passive magnetic shielding device, which is the focus of this article. A beam of circular polarization pumped light irradiates the alkali metal gas chamber in the direction of the Z-axis and the alkali metal atoms generate polarization in the gas chamber. In the action of the magnetic field, the spin-polarized alkali metal atoms produce the larmor precession. A beam of line polarization detection light detects the puller intake of alkali metal atoms in the X-axis direction. The larmor precession frequency is proportional to the strength of the external magnetic field, thus measuring the strength of the magnetic field [22].

D. MODEL ESTABLISHMENT

In order to analyze the change trend of remanence in the magnetic shielding barrel, two simplified finite element models are established and analyzed. Equation (6) contains the size parameters that affect the shielding coefficient of the magnetic shielding barrel.

The size of the magnetic shielding barrel is shown in Table 1 and Table 2.

In FIGURE. 3 and FIGURE. 4, the sectional views of four-layer of cylindrical magnetic shielding barrel and four-layer of spindle magnetic shielding barrel are respectively shown. In practical application, the magnetic shielding device for passive shielding SERF magnetometer needs to open several ports to provide pumping light, detection light, wire, and other channels. This model is built in the presence of these openings, and the material of the magnetic shielding barrel

TABLE 2. Size parameters of the spindle magnetic shield barrel.

Parameter name	Parameter value
Innermost side wall length	159.6 mm
Innermost side wall difference	6.6 mm
Innermost total axis length	250 mm
Innermost radius	65 mm
Total axial length difference between two adjacent layers	10 mm
Radius difference between two adjacent layers	10 mm
Layer thickness	0.4 mm
Number of layers	4

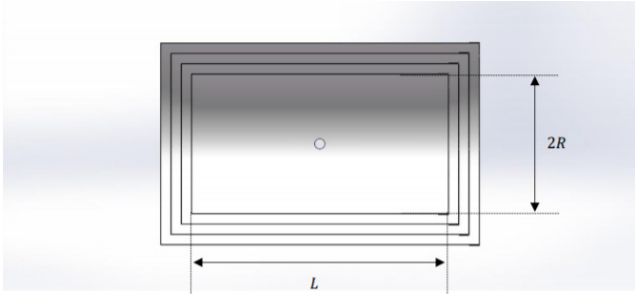

FIGURE 3. Sectional view of four-layer cylindrical magnetic shield barrel.

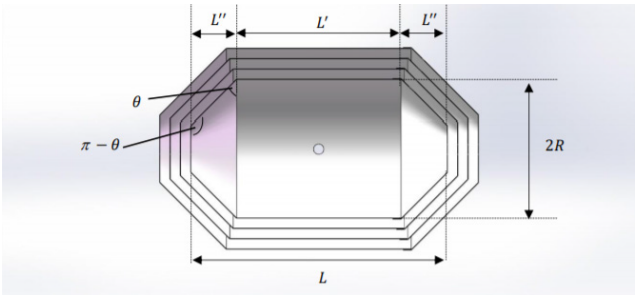

FIGURE 4. Sectional view of four-layer spindle-shaped magnetic shield barrel.

is mu-metal. Maximum permeability μ_{m} is about 250000 mH/m.

The axial shielding coefficient S_a of single-layer spindle shaped magnetic shielding barrel is:

$$S_a \approx \frac{(1+4NS_t)}{(1+\frac{(\frac{L'}{L}R+2\frac{L''}{L}R\sin\theta)}{L})} \tag{8}$$

where: R is the average value of R_{in} and R_{out}, L is the total inner length of single-layer magnetic shielding barrel, N is the demagnetization factor, L' is the length of the cylindrical part, L'' is the length of the spindle part, θ is the angle between the spindle part and the cylindrical part.

E. GEOMAGNETIC FIELD SIMULATION

In this simulation experiment, three-dimensional Helmholtz coil is used to simulate the geomagnetic environment. According to the parameters setting in the three-dimensional

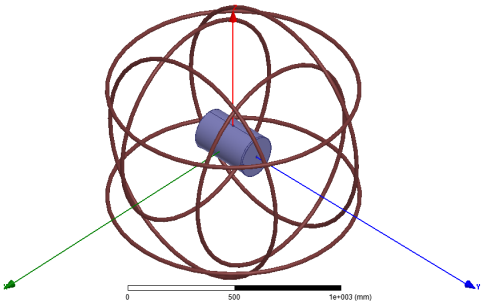

FIGURE 5. Three-dimensional finite element model of four-layer cylindrical magnetic shielding barrel.

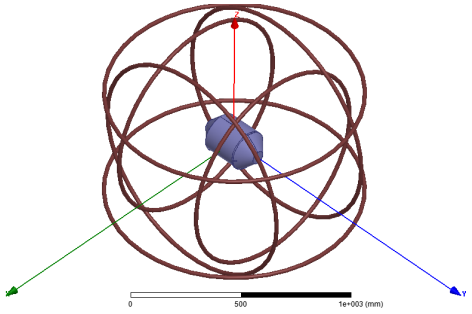

FIGURE 6. Three-dimensional finite element model of four-layer spindle shaped magnetic shielding barrel.

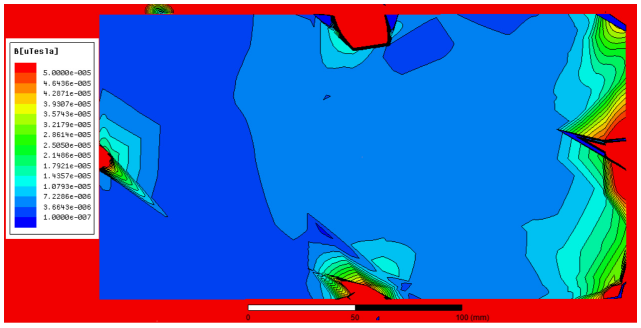

FIGURE 7. Simulation results of axial section magnetic field distribution of the innermost layer of four-layer cylindrical magnetic shielding barrel.

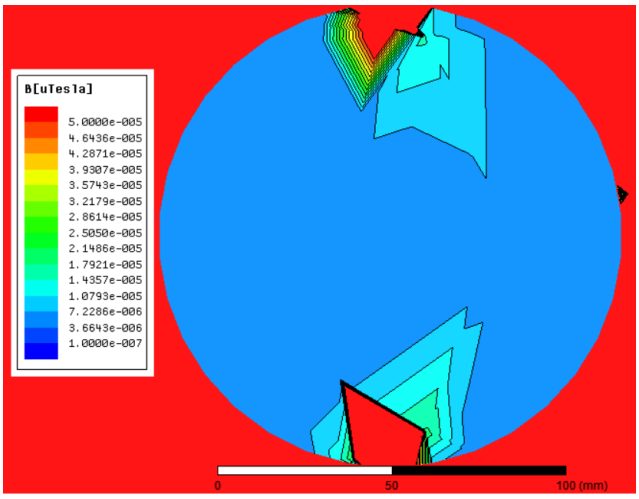

FIGURE 8. Simulation results of magnetic field distribution in the innermost transverse section of four-layer cylindrical magnetic shielding barrel.

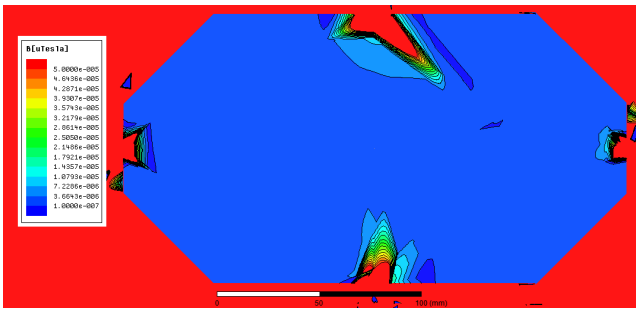

FIGURE 9. Simulation results of magnetic field distribution of axial section in the innermost layer of four-layer spindle magnetic shielding barrel.

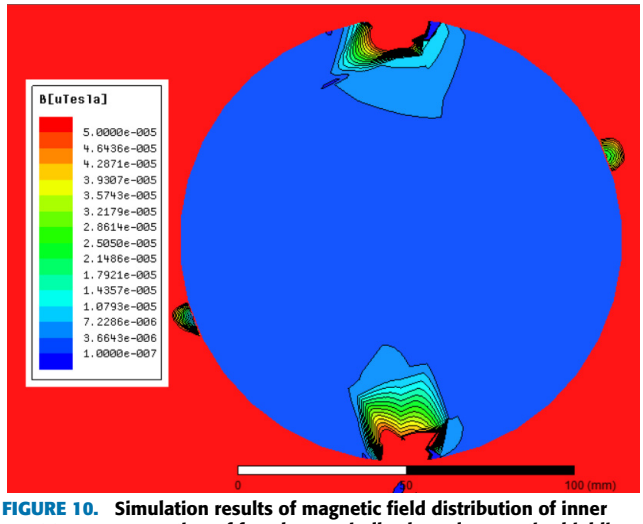

FIGURE 10. Simulation results of magnetic field distribution of inner most transverse section of four-layer spindle shaped magnetic shielding barrel.

coil, 48.323μT magnetic field can be generated at the center point.

The shielding performance of two kinds of magnetic shielding barrels are verified by experiment and simulation. As shown in FIGURE. 5 and FIGURE. 6, in order to make the residual magnetism in the barrel as small as possible, it is necessary to place the through hole towards the Y-axis and the vacuum hole towards the Z-axis.

III. EXPERIMENTAL RESULT

After setting the boundary conditions and excitation sources, we obtain the final magnetic shielding simulation results.

As shown in FIGURE.7 and FIGURE.8, the magnetic field distribution of the innermost axial section and transverse section of the four-layer cylindrical magnetic shielding barrel is shown respectively.

As shown in FIGURE.9 and FIGURE.10, the magnetic field distribution of the innermost axial section and transverse section of the four-layer spindle shaped magnetic shielding barrel is shown respectively.

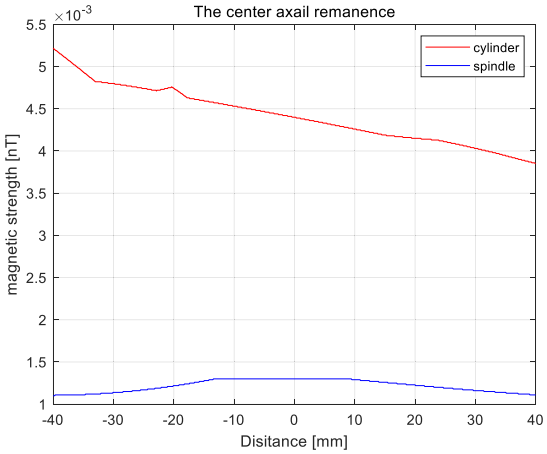

FIGURE 11. Axial remanence curve in the center area of the innermost layer of the magnetic shield barrel. When the layer thickness is 0.4mm.

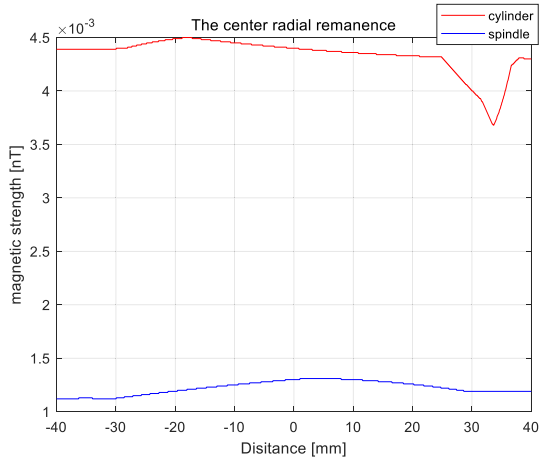

FIGURE 12. Radial remanence curve in the center area of the innermost layer of the magnetic shield barrel. When the layer thickness is 0.4mm.

The shield barrel is made of high magnetic conducting material. The shortest path of magnetic resistance leads to the enrichment of magnetic field in the position of light passing hole, therefore its magnetic induction intensity is stronger than the environmental magnetic field. However, with the increase of the number of layers of the shielding barrel, the magnetic field lines inside the magnetic shielding would be less and less. The uneven distribution of remanence in the magnetic shielding barrels may be caused by the holes in the barrel cover for placing wires and the lack of accuracy of the software and the computer. From the radial and axial cross-sections, the spindle-shaped magnetic shielding barrel has better shielding effect and more uniform internal remanence. Especially in the axial section, the spindle-shaped magnetic shielding barrel has a better shielding effect near the lid due to its shape advantage.

The magnetic shielding effectiveness S_E of the cylindrical magnetic shield barrel is 140.8 and the spindle-shaped magnetic shield barrel is 151.4. As shown in FIGURE.11 and FIGURE.12, it can be seen from the experimental results that the shielding effect of the spindle-shaped magnetic shield barrel is significantly better than that of the cylindrical magnetic shield barrel.

Because of the motion of the electrons, shielding barrels made of mu-metal mainly produce Johnson noise. Noise is related to the radius, thickness, length and diameter ratio and temperature of the shielding barrel. In the innermost shield, the noise produced by the two shielding barrels is basically the same. When the radius of the shielding barrel is 60 cm and the temperature is 330K, the noise generated by both magnetic shielding barrels is about 15fT / $Hz^{1/2}$.

IV. CONCLUSION

The highly sensitive measurement of SERF has a high requirement for magnetic shielding. The effect of magnetic shielding depends on the structure design of the device to a great extent on the premise that the magnetic material is consistent with its processing technology. The remanence of the high performance magnetic shielding barrel at the center is very important for the super sensitive measurement of SERF. In this article, by means of magnetic shielding model calculation and finite element analysis, a spindle shaped magnetic shielding barrel is studied. Compared with the traditional cylindrical magnetic shielding, the shielding effect in the central area is equivalent. In the process of manufacturing, the volume is about 1 / 5 smaller and the weight is about 1 / 4 smaller. At the same time, it has the advantages of good shielding performance, large volume, light weight, low cost, and more efficiency.

REFERENCES

[1] D. M. Miles, I. R. Mann, and M. Ciurzynski, "A miniature, low-power scientific fluxgate magnetometer: A stepping-stone to cube-satellite constellation missions," *J. Geophys. Res-Space Phys.*, vol. 121, no. 12, p. 11,839-11,860, 2016.

[2] Z. Wu and W. Wang, "INS/magnetometer integrated positioning based on neural network for bridging long-time GPS outages," *GPS Solutions*, vol. 23, no. 3, Jul. 2019.

[3] J. K. Sandhu, T. K. Yeoman, M. K. James, I. J. Rae, and R. C. Fear, "Variations of high-latitude geomagnetic pulsation frequencies: A comparison of Time-of-flight estimates and IMAGE magnetometer observations," *J. Geophys. Res., Space Phys.*, vol. 123, no. 1, pp. 567–586, Jan. 2018.

[4] J. Kawai, M. Miyamoto, M. Kawabata, M. Nosé, Y. Haruta, and G. Uehara, "Characterization and demonstration results of a SQUID magnetometer system developed for geomagnetic field measurements," *Superconductor Sci. Technol.*, vol. 30, no. 8, Aug. 2017, Art. no. 084002.

[5] Z. Liu, M. Pan, Y. Tang, Q. Zhang, Y. Geng, C. Wan, D. Chen, and W. Tian, "A new method for distortion magnetic field compensation of a geomagnetic vector measurement system," *Meas. Sci. Technol.*, vol. 27, no. 12, Dec. 2016, Art. no. 125005.

[6] S. Knappe, O. Alem, D. Sheng, and J. Kitching, "Microfabricated optically-pumped magnetometers for biomagnetic applications," *J. Phys., Conf. Ser.*, vol. 723, Jun. 2016, Art. no. 012055.

[7] J. Brew and M. J. Holzinger, "Probabilistic resident space object detection using archival THEMIS fluxgate magnetometer data," *Adv. Space Res.*, vol. 61, no. 9, pp. 2301–2319, May 2018.

[8] H. B. Dang, A. C. Maloof, and M. V. Romalis, "Ultrahigh sensitivity magnetic field and magnetization measurements with an atomic magnetometer," *Appl. Phys. Lett.*, vol. 97, no. 15, Oct. 2010, Art. no. 151110.

[9] E. Boto, S. S. Meyer, V. Shah, O. Alem, S. Knappe, P. Kruger, T. M. Fromhold, M. Lim, P. M. Glover, P. G. Morris, R. Bowtell, G. R. Barnes, and M. J. Brookes, "A new generation of magnetoencephalography: Room temperature measurements using optically-pumped magnetometers," *NeuroImage*, vol. 149, pp. 404–414, Apr. 2017.

[10] S. J. Seltzer, *Developments in Alkali—Metal Atomic Magnetometry*. Ann Arbor, MD, USA: Princeton Univ., 2008.

[11] J. Zhao, M. Ding, J. Lu, K. Yang, D. Ma, H. Yao, B. Han, and G. Liu, "Determination of spin polarization in spin-exchange relaxation-free atomic magnetometer using transient response," *IEEE Trans. Instrum. Meas.*, vol. 69, no. 3, pp. 845–852, Mar. 2020.

[12] J. Zhang, M. Ding, Y. Hu, H. Yao, D. Ma, J. Cai, J. Lu, and B. Han, "A novel asymmetrical heating method for improving the temperature spatial homogeneity of vapor cell in atomic magnetometer," *IEEE Access*, vol. 7, pp. 71245–71251, 2019.

[13] J. Zhao, G. Liu, J. Lu, K. Yang, D. Ma, B. Xing, B. Han, and M. Ding, "A non-modulated triaxial magnetic field compensation method for spin-exchange relaxation-free magnetometer based on zero-field resonance," *IEEE Access*, vol. 7, pp. 167557–167565, 2019.

[14] G. Wojciech and S. Pustelny, "Optical Magnetometry," *Photon. Lett. Poland*, vol. 1, p. 34, Jan. 2009.

[15] S. Kuriki, A. Hayashi, T. Washio, and M. Fujita, "Active compensation in combination with weak passive shielding for magnetocardiographic measurements," *Rev. Sci. Instrum.*, vol. 73, no. 2, pp. 440–445, Feb. 2002.

[16] J. Lu, D. Ma, K. Yang, W. Quan, J. Zhao, B. Xing, B. Han, and M. Ding, "Study of magnetic noise of a multi-annular ferrite shield," *IEEE Access*, vol. 8, pp. 40918–40924, 2020.

[17] S.-K. Lee and M. V. Romalis, "Calculation of magnetic field noise from high-permeability magnetic shields and conducting objects with simple geometry," *J. Appl. Phys.*, vol. 103, no. 8, Apr. 2008, Art. no. 084904.

[18] T. W. Kornack, S. J. Smullin, S.-K. Lee, and M. V. Romalis, "A low-noise ferrite magnetic shield," *Appl. Phys. Lett.*, vol. 90, no. 22, May 2007, Art. no. 223501.

[19] K. Hogan, J.-F. Fagnard, L. Wéra, B. Vanderheyden, and P. Vanderbemden, "Magnetic shielding of an inhomogeneous magnetic field source by a bulk superconducting tube," *Superconductor Sci. Technol.*, vol. 28, no. 3, Mar. 2015, Art. no. 035011.

[20] S. Di Fraia, M. Marracci, B. Tellini, and C. Zappacosta, "Shielding effectiveness measurements for ferromagnetic shields," *IEEE Trans. Instrum. Meas.*, vol. 58, no. 1, pp. 115–121, Jan. 2009.

[21] K. Tashiro, H. Wakiwaka, K. Matsumura, and K. Okano, "Desktop magnetic shielding system for the calibration of high-sensitivity magnetometers," *IEEE Trans. Magn.*, vol. 47, no. 10, pp. 4270–4273, Oct. 2011.

[22] J. Li, W. Quan, B. Han, F. Liu, L. Xing, and G. Liu, "Multilayer cylindrical magnetic shield for SERF atomic co-magnetometer application," *IEEE Sensors J.*, vol. 19, no. 8, pp. 2916–2923, Apr. 2019.

[23] D. Budker and M. Romalis, "Optical magnetometry," *Nature Phys.*, vol. 3, pp. 227–234, Apr. 2007.

[24] T. J. Sumner, J. M. Pendlebury, and K. F. Smith, "Convectional magnetic shielding," *J. Phys. D, Appl. Phys.*, vol. 20, no. 9, pp. 1095–1101, Sep. 1987.

[25] A. Mager, "Magnetic shielding efficiencies of cylindrical shells with axis parallel to the field," *J. Appl. Phys.*, vol. 39, no. 3, p. 1914, Feb. 1968.

[26] K. Yang, J. Lu, M. Ding, J. Zhao, D. Ma, Y. Li, B. Xing, B. Han, and J. Fang, "Improved measurement of the low-frequency complex permeability of ferrite annulus for low-noise magnetic shielding," *IEEE Access*, vol. 7, pp. 126059–126065, 2019.

[27] D. Ma, M. Ding, J. Lu, H. Yao, J. Zhao, K. Yang, J. Cai, and B. Han, "Study of shielding ratio of cylindrical ferrite enclosure with gaps and holes," *IEEE Sensors J.*, vol. 19, no. 15, pp. 6085–6092, Aug. 2019.

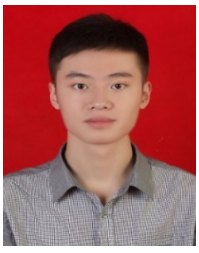

ZHENGKUN FAN was born in Lanzhou, Gansu, China, in 1995. He received the B.E. degree from the School of Optoelectronic Information and Computer Engineering, University of Shanghai for Science and Technology, China, in 2018, where he is currently pursuing the M.S. degree. His main research interests include the design of high-performance shielding cylinders, weak magnetic field detection, and atomic magnetometer research.

JUN XU received the B.E. degree from Jiangsu Ocean University, in 2016. He is currently pursuing the Ph.D. degree with the School of Optical-Electrical and Computer Engineering, University of Shanghai for Science and Technology. His current research interests include magnetic field compensation, magnetic field coil design, and atomic magnetometer.

XIANGYU KANG was born in Linyi, Shandong, China, in 1995. He received the B.E. degree from the School of Computer and Control Engineering, Yantai University, in 2018. He is currently pursuing the M.S. degree with the School of Optoelectronic Information and Computer Engineering, University of Shanghai for Science and Technology. His major research interests include weak magnetic signal detection, magnetic field active compensation, and atomic magnetic field control.

ZHANFEI ZHANG was born in Guizhou, China, in 1997. He is currently pursuing the B.E. degree with the School of Optoelectronic Information and Computer Engineering, University of Shanghai for Science and Technology. His research interests include weak magnetic field detection and atomic magnetometer research.

YANG LI received the Ph.D. degree from Beihang University, in 2019. He is currently a Lecturer with the University of Shanghai for Science and Technology. His current research interest includes hybrid optical pumping atomic magnetometer.

XIANGMEI DONG received the B.S. degree from Henan Polytechnic University, China, in 2000, and the M.S. and Ph.D. degrees from the University of Shanghai for Science and Technology (USST), China, in 2005 and 2012, respectively. She currently works with USST. Her current research interests include smart sensing technology, optical engineering, optical imaging, and magneto-optical effect.

XIUMIN GAO was born in 1978. He received the Ph.D. degree from the Shanghai Institute of Optics and Fine Mechanics (SIOM), in 2006. He joined the University of Shanghai for Science and Technology, in 2017. He is currently a Leader of several research programs, including the National Natural Science Foundation of China and the National Key Research and Development Plan. He has published more than 60 articles in journals, such as *Nature Communications*, *Scientific Reports*, and *Applied Optics*. His current research interests include instruments and meters, smart sensing technology, optical engineering, atomic magnetometer, and precision measurement.